Evidence for a disorder driven phase transition in the condensation of 4He in aerogels

Fabien Bonnet, Thierry Lambert, Benjamin Cross, Laurent Guyon, Florence Despetis, Laurent Puech, Pierre-Etienne Wolf

Evidence for a disorder driven phase transition in the condensation of ^{4}He in aerogels

F. Bonnet[1], T. Lambert[1], B. Cross[1], L. Guyon[1], F. Despetis[2], L. Puech[1] and P.E. Wolf[1]

[1] *Institut Néel, CNRS/UJF, BP 166, 38042 Grenoble-Cedex 9, France*
[2] *Groupe d'Etude des Semiconducteurs, CNRS-UMR 5650, Université Montpellier II Case Courrier 074, 34095 Montpellier-Cedex 5, France*

PACS 64.60.-i – General studies of phase transitions
PACS 64.70.F- – Liquid-Vapour transitions
PACS 67.25.bh – Quantum fluids and solids : ^{4}He - Films and restricted geometries.

Abstract. - We report on thermodynamic and optical measurements of the condensation process of ^{4}He in three silica aerogels of different microstructures. For the two base-catalysed aerogels, the temperature dependence of the shape of adsorption isotherms and of the morphology of the condensation process show evidence of a disorder driven transition, in agreement with recent theoretical predictions. This transition is not observed for a neutral-catalysed aerogel, which we interpret as due to a larger disorder in this case.

Introduction. – The liquid-gas transition of a bulk fluid is an archetypal example of a first order transition. Condensation and evaporation of fluids in various porous media have thus been widely studied in order to understand the influence of confinement on such transitions. When the pressure is increased at a constant temperature, the general picture, in the case where the liquid phase wets the substrate, is a progressive adsorption of a thin dense film at low vapour pressure, followed by a rather abrupt filling below the saturated vapour pressure. This phenomenon is ascribed to capillary effects and is denominated capillary condensation. In the classical picture, the difference between the filling pressure and the bulk saturation pressure decreases with increasing pore size, and the range of pressures over which the condensation takes place reflects the pores size distribution. A characteristic of the capillary condensed regime is the hysteresis between condensation and evaporation. The porous medium empties at a lower pressure than it fills, resulting in an hysteresis loop in the plane pressure-(average) fluid density. This behaviour can have different origins. In the case of disconnected pores (as in controlled-pore glasses, e.g. MCM41 silica), it can be interpreted in terms of the change of the meniscus shape between filling and emptying [1]. For a network of connected pores of different sizes (e.g., in Vycor silica glass), it is believed to stem from the energy barrier for nucleating a liquid vapour interface. A pore cannot empty as long as its smaller neighbours remain filled, so that emptying involves a specific percolation process [2].

Recent numerical studies, based on a mean-field density functional theory, shed a new light on capillary condensation [3, 4]. A central point is that hysteresis results from the energetic and geometric disorder of the porous media. As in disordered magnetic systems [5],

disorder induces a complex free-energy landscape, resulting in a large number of metastable equilibrium states, corresponding to different configurations of the microscopic liquid-vapour interface. If thermal fluctuations are negligible, the system remains trapped in one minimum as the pressure is increased (or decreased), up to the point where this minimum disappears and the system moves to another minimum, corresponding to an avalanche where some region of the porous material transits from vapour to liquid (or reversely). The state of the system then depends on its history, whence hysteresis.

These studies predict the existence of a disorder-driven transition similar to that occurring in the Random Field Ising Model at zero temperature [5]. At small porosity $\mathcal{P}$ (or large disorder), filling takes place by a succession of small, microscopic avalanches. The maximal size of the avalanches increases with $\mathcal{P}$, up to some critical value $\mathcal{P}_c$ (corresponding to some critical disorder), where it diverges. Above $\mathcal{P}_c(T)$, which increases with increasing temperature T, filling involves a macroscopic avalanche, associated with a jump in the average fluid density, at some well defined pressure. This out-of-equilibrium phase transition implies a change of shape, from smooth to steep, of the condensation branch of the hysteresis loop, when the porosity is increased at a constant temperature or, alternatively, when the temperature is decreased below some critical value, at a constant porosity [6]. In magnetic systems, an equivalent change of the hysteresis loop has been observed in Co/CoO disordered films [7].

Such a change as a function of temperature is not observed in Vycor and other usual porous materials. In the new theoretical approach, it implies that the disorder in these materials is larger than its critical value at zero temperature. Thus, a clear demonstration of the specific role of disorder requires to find a material where the disorder is small enough to observe the out-of-equilibrium phase transition at a finite temperature. Ideal candidates are silica aerogels, where the silica forms a complex arrangement of interconnected strands. Their porosity is large and can be varied in a wide range (up to 99%, and more), offering an experimental, free-standing, realisation of weak and tunable disorder. Furthermore, most of the recent theoretical studies have been performed on aerogels numerically synthesised by Diffusion Limited Cluster Aggregation, which mimics real aerogels synthesised under basic conditions. These numerical studies predict that, for 87% porosity aerogels, avalanches are always microscopic, while, for 95% porosity aerogels, a transition from microscopic to macroscopic avalanches takes place at a finite temperature.

Earlier experiments on condensation of helium inside aerogels offer indeed some support for the new scenario. Excepting the first ones [8], experiments carried out by different groups on similar aerogels (95% porosity, gelation process with basic pH), show that, as in other porous materials, sorption isotherms are hysteretic, and that condensation occurs over a finite range of pressures [9–12]. Still, this range seems unexpectedly narrow, considering the disordered structure of the silica strands, especially at large porosity (i.e. weak disorder) [9, 12] or low temperature [11, 12]. Steep isotherms have also been measured using nitrogen as a fluid, but, here, the situation is made complex by the large contraction of the compliant gels upon adsorption [13]. This problem does not arise with helium, thanks to its much lower surface tension [14].

The aim of the experiments reported here was to further investigate the adequacy of the disorder-driven scenario, using combined optical and thermodynamic measurements to study the effect of temperature on condensation in three aerogels of different microstructures and porosities.

Experimental. – Studied aerogels are B100, N102, and B55, where the letter corresponds to the pH during synthesis (basic or neutral), and the number to the density (in kg/m^3). We synthesised B100 and N102 (of porosities $\mathcal{P}$=95.5%) using a one step process [15], while B55 ($\mathcal{P}$ =97.5%) has been synthesised at NorthWestern University by J. Pollanen using a two-step process. Aerogels have a fractal structure (characterised by a fractal dimension D_f) between the size a of building silica units and a correlation length

ξ_G. From previous neutron and X-ray scattering experiments on similar samples, we expect that D_f and ξ_G are similar for B100 [16, 17] and B55 [18] (1.7 and 10 nm ± 20%), and larger for N102 [19] (2.6 and 20 nm ± 20%). Since $\mathcal{P} \propto (\xi_G/a)^{3-D_f}$, both N102 and B55 must have a fractal range ξ_G/a larger than B100. We directly measured ξ_G for our samples using light scattering. This gives the structure factor $S(q)$ at zero q, which depends on $\mathcal{P}$, D_f, and ξ_G [20]. The measured $S(0)$ corresponds to a light mean free path of 3.5 mm for N102, 50 mm for B100 and 100 mm for B55. Using the above D_f and $\mathcal{P}$ values, this yields ξ_G values within 20% of those expected from the SANS and SAXS measurements. In particular, the stronger scattering for N102 reflects its larger ξ_G.

Aerogels were grown as cylinders (14 mm in diameter for B100 and N102, 10 mm for B55), from which we sliced thin disks (2.7 mm thick for B100, 4 mm thick for N102 and B55) to fit into a 4 mm thick copper experimental cell closed by two sapphire windows. The cell was mounted in a cryostat with 8 optical ports 45 ° apart, allowing observation of samples under different scattering angles. Sorption isotherms were performed on these samples between 4.2 K and the critical bulk temperature. The pressure in the cell was measured as a function of the injected helium amount, and simultaneous light scattering measurements were performed to probe the distribution of helium inside the aerogels. Except for N102 (due to its strong intrinsic scattering), the level of multiple scattering was generally weak. This is a specific advantage of the low index of refraction of helium (1.024 at 4.2 K).

The flow in or out from the cell was controlled with a regulated flowmeter for B100 and N102, and by changing the temperature of an external reservoir connected to the cell for B55 [21]. The flowrate must be small enough that the heat released by the condensation process creates a negligible temperature gradient inside the aerogel. For B100 and N102, the filling time corresponding to the hysteretic part of the adsorption isotherm was between 15 to 30 hours, which we checked to be long enough. For B55, it ranged from 6 to 48 hours.

The helium mass in the aerogel is obtained by integrating the flowrate over time (for B100 and N102) or from the temperature of the reservoir (for B55), and correcting for cold and warm dead volumes [11]. Conversion of this mass into a condensed fraction Φ must take into account the compression of the helium close to the silica, especially for temperatures close to the bulk critical point. We thus impose Φ=1 for the filled aerogel (i.e. zero vapour fraction) and compute the change of Φ from the change in mass from this initial point, assuming that the density of the dense phase and of the vapour inside the aerogel both have their bulk value [11]. The result will be correct as long as the first layers of helium are not affected, i.e. except for small fractions.

Results. – Isotherms for the three samples are shown in figs. 1 and 2a. Figure 1 compares the isotherms obtained for B100 and N102. The general trends are in qualitative agreement with the usual picture of capillary condensation; the hysteresis loop gets narrower and closer to the bulk saturation pressure P_{sat} as the surface tension decreases with increasing temperature. Also, it is smoother, and closer to P_{sat} for N102, consistent with the wider distribution of pores extending up to larger sizes.

We quantify the position of the adsorption isotherm by $\Delta P = P_{max} - P_{sat}$, where P_{max} is the pressure where its slope is the largest. For a cylindrical pore of radius R, filling occurs at the stability limit of the adsorbed film. For R much larger than the film thickness, this gives [22, 23] $\Delta P = \rho_V/(\rho_L - \rho_V).\sigma/R$, where σ is the helium surface tension, and ρ_L and ρ_V are the bulk liquid and vapour densities at saturation. For a collection of independent pores, ΔP corresponds to the average pore size. Although, *a priori* , aerogels cannot be so simply described, fig. 2b shows that the equation above accounts for the temperature dependence of ΔP for N102 in the whole temperature range, and for B100 above 4.95 K, with characteristic 'pores' sizes $R \simeq 35$ nm and 20 nm. Both values are about twice the measured correlation lengths. For the larger porosity sample B55, ΔP is affected by the flowrate used, due to the heating effect of adsorption, but the error is small, as shown by the point for a slow filling at 4.89 K. We estimate the corresponding average pore size to

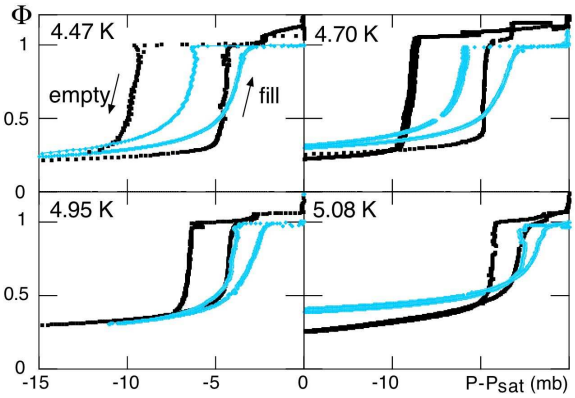

Fig. 1: Hysteresis loops at four temperatures, 4.47, 4.71, 4.96 and 5.08 K, for two aerogels of porosity 95%, B100 (black) and N102 (grey). The liquid fraction Φ in aerogel is plotted versus $P - P_{sat}$, where P_{sat} varies between 1260 and 2090 mb; for B100, there is a clear change of shape with temperature.

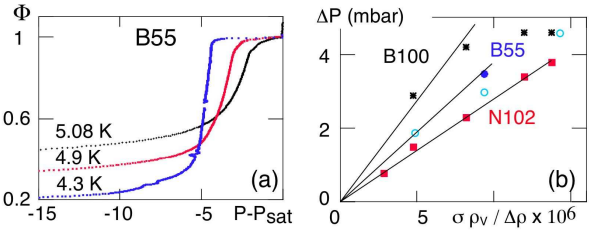

Fig. 2: a) B55 raw adsorption isotherms for a 0.2 STP cc/min flowrate, corresponding to a filling time of order 12 hours; b) Position ΔP of the point of the condensation branch with maximal slope versus the temperature dependent ratio $\sigma\rho_V/(\rho_L - \rho_V)$ (in J/m^2) for the different samples. For B55, the filling time is 12 h for the open circles and 48 h for the closed one. The straight lines correspond to average pore diameters of 18, 25, and 36 nm.

be 25 nm, intermediate between B100 and N102. Comparison of B100 and N102 show that the average pore size at constant porosity increases with the gel correlation length ξ_G, while comparison of B100 and B55 shows that, at given ξ_G, it depends on porosity. In other words, both the porosity and the correlation length influence the position of the isotherms.

For both B100 and B55, the isotherms are steeper at low than at large temperatures. This is inconsistent with the usual picture of capillary condensation, where the shape of the isotherms reflects the pore distribution.

This is not an effect of adsorption. For a flat substrate, the film thickness at ΔP, being proportional to $((\rho_L - \rho_V)/\sigma)^{1/3}$, increases with temperature. This also holds for a cylindrical pore [23]. We thus expect that the fraction Φ_0 at the lower closure point of the hysteresis loop increases with temperature, which is in agreement with fig. 1. In order to take into account this effect when comparing the isotherms between different temperatures, we transform Φ to $\tilde{\Phi}=(\Phi-\Phi_0)/(1-\Phi_0)$, the condensed fraction excluding the film. We also normalise the pressure axis by ΔP, to account for the different average pores sizes and the temperature dependence of σ and $\rho_L - \rho_V$. Figure 3 shows that the thus normalized isotherms collapse for N102. This is consistent with the usual picture of capillary condensation, where the spatial distribution of liquid (hence the interface curvature, to which the pressure is related through Kelvin's equation), only depends on the condensed fraction, not on the temperature. In contrast, such a picture breaks down for the base-synthetised samples, for

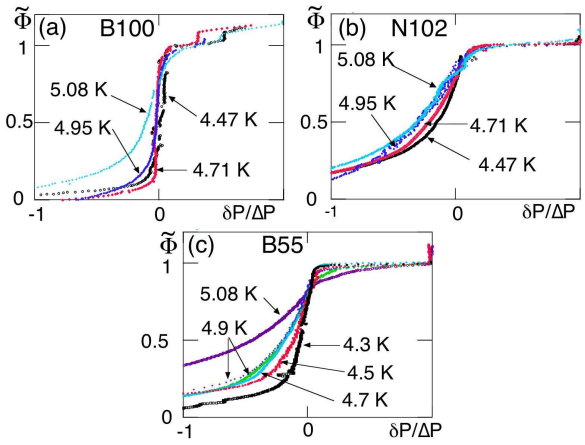

Fig. 3: Normalised isotherms for B100 (a), N102 (b), and B55 (c). The abscissa is $\delta P = P - P_{max}$ normalized by ΔP, which equals 1 at P_{sat}. $\tilde{\Phi}$ is the condensed fraction excluding the adsorbed film (see text). For B55, flowrates range between 0.05 and 0.4 STPcc/min. Although ΔP at 4.9 K depends on the flowrate, the normalized isotherm does not. The temperature dependence for B100 is consistent with a disorder driven transition occurring occurring between 4.71 K and 4.95 K.

which the isotherms become steeper at low temperature. The behaviour for these samples supports the scenario of a disorder-driven transition. For B100, the normalized isotherm is nearly vertical for 4.47 K and 4.71 K, implying that the critical temperature lies between 4.71 K and 4.95 K. Although there is no corresponding theoretical prediction, this transition might also cause the anomalous behaviour of ΔP below 4.95 K. For B55, the isotherms are less steep than for B100, and the effect of temperature is not as pronounced. This is surprising as measurements by Herman *et al* show a much steeper isotherm for a 97.5% sample than for a 95% sample, both one-step synthesised. The smoother isotherms for our B55 could result either from a broadening caused by large heterogeneities of the average silica density, or from the different microstructure induced by the two-step synthesis.

We now come to the optical measurements. We illuminate the aerogel by a thin (100 μm wide), vertically polarised, He-Ne laser sheet under a 45° incidence with respect to its faces, and image it at 45°, 90°, and (for N102 and B55) 135° using CCD cameras. At any point of the intercept of the aerogel by the laser sheet, the brightness of the image is proportional to the intensity scattered in the direction of observation. The upper part of fig. 4 shows images of B100 for increasing helium fractions along the adsorption isotherms, and fig. 5 the scattered intensity by the three selected spots in the images. Quantitative analysis of these curves show that, below $\Phi \approx 0.3$, the scattered intensity is that expected for a thin film of helium covering uniformly the silica strands, whereas, beyond this value, it becomes much larger, implying the formation of liquid clusters correlated over distances larger than the correlation length of the silica [11]. Strikingly, while this increase of the scattered intensity occurs uniformly over the sample for the two larger temperatures, for the two lower ones, it is only so for fractions less than about 0.5. Beyond, liquid progressively invades the aerogel, resulting in the growth of dark regions. Since the macroscopic morphology is identical for 4.47 K and 4.71 K, and for different rates of condensation as well, it must reflect macroscopic, heterogeneities of the average density of silica, which make some regions favour slightly more the liquid. The fact that the filling pattern is homogeneous above 4.95 K then implies that the isotherm intrinsic width is larger than its broadening due to the heterogeneities, the reverse being true below 4.95 K. The observed change of morphology is thus a signature of the change of slope of the isotherm.

These observations exhibit the behaviour expected for macroscopic avalanches; at any

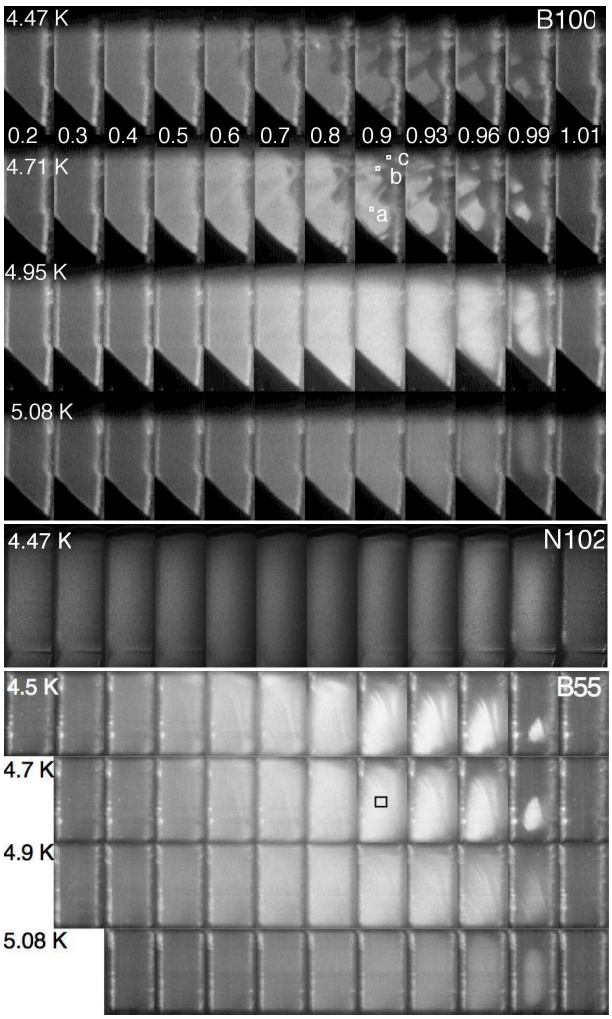

Fig. 4: Images observed at 45° from the incident laser sheet for condensed fractions from 0.2 to 0.9 (by steps of 0.1), 0.93, 0.96, 0.99 and 1.01. The width of the images is 4 mm; top panel : B100 (logarithmic grey scale); middle panel : N102 at 4.47 K (linear grey scale); bottom panel : B55 (logarithmic gray scale). The rectangles for B100 and B55 are those used to measure the intensity in figs. 5 and 7.

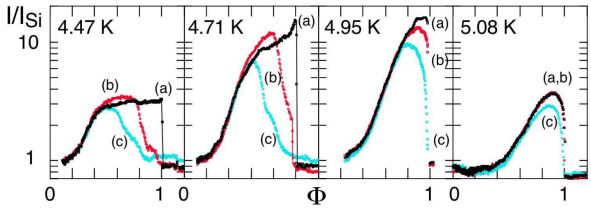

Fig. 5: Scattered intensity for B100, referred to the empty aerogel situation, for the three regions labelled (a), (b), (c) in fig. 4a. The smaller scattering at low temperature points to a temperature dependence of the microscopic distribution of liquid at a given condensed fraction Φ.

given spot, the transition to the dark state occurs discontinuously, when this spot is swept by the boundary between the bright and the dark regions. This is consistent with the

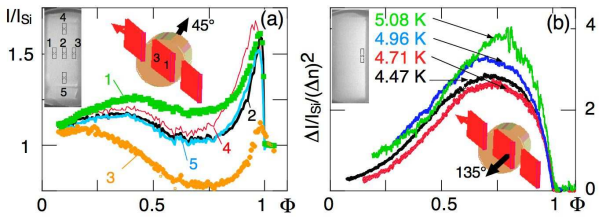

Fig. 6: Intensity scattered by N102 as a function of the condensed fraction Φ : a) at 4.47 K and 45°. The signal, normalized by the silica contribution, corresponds to five regions at three different depths inside the aerogel disk. Differences between curves are consistent with multiple scattering effects combined with an homogeneous distribution of the liquid clusters within the sample, in contrast to B100 at the same temperature; b) at 135°, close to the entrance of the laser sheet. The silica contribution I_{Si} has been subtracted, and the result normalized by I_{Si} and $(\Delta n(T)/\Delta n(4.47))^2$, the square of the optical contrast Δn normalized to its value at 4.47 K. The signal is similar at all temperatures, suggesting that, unlike for B100, the spatial distribution of the liquid does not depend on temperature.

occurrence of a macroscopic (but local) avalanche from a partly filled to a fully filled state. This will make the pressure at which the avalanche takes place to vary continuously in space, so that the transition should occur successively at different locations in the aerogel, in qualitative agreement with the observations.

Thus, the results for B100 lead us to suggest that this sample exhibits a disorder induced transition, which the change of filling pattern would be another marker of. The relationship between the filling pattern and the shape of the isotherms is supported by the behaviour observed for N102 at 4.47 K in fig. 4. Due to the strong scattering of the aerogel, the images are blurred, but do not show any sign of heterogeneity except very close to filling, consistent with the fact that the isotherm is smooth even at this temperature. The homogeneity of the filling pattern is confirmed by the quantitative analysis of fig. 6(a) : at any fraction Φ, the intensity scattered at 45° is the same along any vertical line of the picture, corresponding to a given depth, hence path length, inside the sample. There is a difference between points at different depths, but this (as well as the bump in the signal at $\Phi \approx 0.4$) can be explained by multiple scattering effects.

For B55, the behaviour resembles that observed for B100. Figure 4 shows heterogeneities in the form of filaments above $\Phi \approx 0.5$, which disappear around 4.89 K. This change of morphology, together with the isotherms of fig. 2, suggests that a disorder driven transition also occurs for this sample. If this is true, the critical temperature would not be very different from that for B100, despite the larger porosity. This, as well as the absence of transition for N102, shows that the pertinent parameter for determining the disorder-induced transition involves not only the porosity, but the whole microstructure.

Another way of demonstrating the disorder driven scenario would be to measure the microscopic distribution of liquid as a function of condensed fraction Φ. Our experiments already allow to compare the size of the correlated helium clusters (droplets or bubbles) between different temperatures and samples. Assuming independent and spherical clusters, the scattered intensity depends on their size and density, or, equivalently, on their size and local liquid (or vapour) volume fraction. For sizes smaller than the wavelength, the Rayleigh-Gans scattering regime applies, and, at a given fraction, the scattered intensity is expected to increase with the size and to be proportional to the contrast factor $(\Delta n)^2$, where Δn is the difference in refractive index between the liquid and the vapour.

Comparison of figs. 5, 6b, and 7a shows different behaviours for the different samples. For B100, the scattered intensity, at a given Φ, is smaller at 4.46 K than at 4.71 K (which is obvious on the images of fig. 4), although the contrast factor is larger. In the low temperature

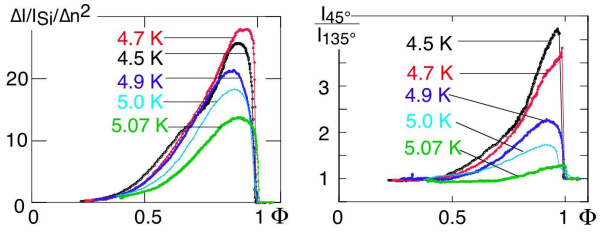

Fig. 7: a) Normalized intensity scattered at 45° by B55 as a function of the condensed fraction Φ. The studied region is the rectangle in fig. 4. The decrease of signal with increasing temperature indicates that the size of correlated domains decreases. b) Anisotropy of scattering between 45° and 135°. Its Φ and temperature dependencies show that the correlated domains size reaches a maximum close to filling, and that the maximal size is larger than 100 nm and decreases with increasing temperature.

regime, the size of liquid clusters thus increases with temperature. In contrast, for N102, once rescaled by the contrast factor, the intensity scattered at 135° close to the entrance of the laser sheet[1] behaves roughly the same, whatever the temperature. This suggests that, at a given Φ, the distribution of liquid does not depend too much on temperature. For B55, the signal is temperature dependent, but does not decrease at low temperature. The low temperature behaviour of B100 thus appears singular, and its origin remains to be understood.

For all samples, the optical signal reaches its maximum between Φ=0.75 and 0.95. In this range, it probably originates from bubbles of vapour. Assuming these bubbles to be spherical, their size can be estimated from the scattered intensity (for the case of homogeneous filling, when the local liquid volume fraction coincides with the measured global fraction Φ), or from the anisotropy of scattering (fig. 7b). Both estimates give a diameter of order 200 to 300 nm for B100 and B55, which tends to decrease with increasing temperature above 4.9 K. For N102, the sharp peak at 45° in fig. 6a also implies a large diameter. Due to the complexity brought by multiple scattering, only a lower bound of about 200 nm can be determined.

Numerical studies of the avalanches size distribution for basic-like aerogels of porosity between 87% and 95% have shown that the avalanches size increases along the adsorption isotherms, to reach a maximum close to filling, and also increases with increasing porosity or decreasing temperature [24]. These predictions cannot be directly compared to our experiments, as we only measure the size of correlated liquid or vapour domains. However, close to Φ=1, one might expect that the avalanches consist in filling the last surviving bubbles. The size decrease of these bubbles with increasing temperature would be qualitatively consistent with the theory. Quantitatively, however, numerical studies predict a size of 1 to 2 ξ_G, depending on temperature, whereas we find bubbles sizes larger than 10 ξ_G. A more direct comparison to theory is possible by using the results of a numerical study on a 87% porosity aerogel at low temperature, the behaviour of which is expected to be similar to a 95% porosity aerogel above its transition temperature [25]. This study predicts that the range of fluid-fluid correlations reaches a maximum of order 2 ξ_G close the point of maximal slope in the isotherm. While the position of this maximum is consistent with our experiments, its value is again lower than the measured size of correlated regions. Further work, both theoretical and experimental, is needed to understand this discrepancy.

Conclusions. – We have shown that different light aerogels behave very differently with respect to adsorption. Our results provide a strong evidence for the occurrence of a

[1]At other positions inside the aerogel, or at 45°, the attenuation due to scattering along the light path does not allow such a direct comparison.

disorder induced transition as a function of temperature in B100. At the same porosity, N102 does not present any transition. In the framework of the disorder-driven transition, this implies a larger disorder in this case, which would come from the wider distribution of length scales for this aerogel. It would be interesting to perform numerical studies on similar aerogels to support this interpretation. In the lighter aerogel B55, there seems to be a transition, but not as clear as for B100. This contrasts with the theoretical expectations and could result either from a less homogeneous sample or from the different microstructure due to the method of synthesis. Checking whether the transition moves to larger temperatures when the porosity increases will therefore require to compare aerogels of different porosities synthesised by the same method. Finally, our experiment demonstrates that optical measurements are a powerful tool, complementary to the isotherms, for the study of adsorption of helium in aerogels, and more generally, in porous media.

* * *

We acknowledge T. Herman, J. Beamish, F. Detcheverry, E. Kierlik, M.L. Rosinberg, G. Tarjus, and J. Phalippou for useful suggestions or discussions. We are grateful to J. Pollanen and W. P. Halperin for providing sample B55 with support from NSF DMR-0703656. Studies on B55 were supported by ANR-06-BLAN-0098.

REFERENCES

[1] Gelb L. D., Gubbins K. E., Radhakrishnan R. and Sliwinska-Bartkowiac M., *Rep.Prog.Phys* , **62** (1999) 1573.
[2] Mason G., *Proc. R. Soc. Lond.* , **415** (1988) 453.
[3] Kierlik E., Monson P. A., Rosinberg M. L., Sarkisov L. and Tarjus G., *Phys. Rev. Lett.* , **87** (2001) 055701.
[4] Sarkisov L. and Monson P., *Phys. Rev. E* , **65** (2001) 011202.
[5] Sethna J. P., Dahmen K., Kartha S., Krumhansl J. A., Roberts B. W. and Shore J. D., *Phys. Rev. Lett.* , **70** (1993) 3347.
[6] Detcheverry F., Kierlik E., Rosinberg M. L. and Tarjus G., *Phys. Rev. E* , **68** (2003) 061504.
[7] Berger A., Inomata A., Jiang J. S., Pearson J. E. and Bader S. D., *Phys. Rev. Lett.* , **85** (2000) 4176.
[8] Wong A. P. Y. and Chan M. H. W., *Phys. Rev. Lett.* , **65** (1990) 2567.
[9] Tulimieri D. J., Yoon J. and Chan M. H. W., *Phys. Rev. Lett.* , **82** (1999) 121.
[10] Gabay C., Despetis F., Wolf P. E. and Puech L., *J. Low Temp. Phys.* , **121** (2000) 585.
[11] Lambert T., Gabay C., Puech L. and Wolf P. E., *J. Low Temp. Phys.* , **134** (2004) 293.
[12] Herman T., Day J. and Beamish J., *Phys. Rev. B* , **72** (2005) 184202.
[13] Reichenauer G. and Scherer G. W., *J. Non-Cryst. Solids* , **285** (2001) 167.
[14] Herman T., Day J. and Beamish J., *Phys. Rev. B* , **73** (2006) 094127.
[15] see e.g. J. Phalippou, Woignier T., Despetis F. and Etienne-Calas S., *Handbook of Sol Gel Science and Technology, Processing Characterization and Applications* Vol. 1 (Kluwer Academic Publishers, Boston) 2005.
[16] Hasmy A., Anglaret E., Foret M., Pelous J. and Jullien R., *Phys. Rev. B* , **50** (1994) 6006.
[17] Wang J., Shen J., Zhou B. and Wu X., *Nanostruct. Mater.* , **7** (1996) 699.
[18] Pollanen J., Choi H., Davis J., Blinstein S., Lippman T., Lurio L., Mulders N. and Halperin W., *AIP Conf. Proc.* , **850** (2006) 237.
[19] Vacher R., Woignier T., Pelous J. and Courtens E., *Phys. Rev. B* , **37** (1988) 6500.
[20] Ferri F., Frisken B. J. and Cannell D. S., *Phys. Rev. Lett.* , **67** (1991) 3626.
[21] Cross B., Puech L. and Wolf P. E., *J. Low Temp. Phys.* , **148** (2007) 903.
[22] Everett D. and Haynes J., *Journal al of Colloid and Interface Science* , **38** (1972) 125.
[23] Saam W. F. and Cole M. W., *Phys. Rev. B* , **11** (1975) 1086.
[24] Detcheverry F., Kierlik E., Rosinberg M. L. and Tarjus G., *Phys. Rev. E* , **72** (2005) 051506.

[25] Detcheverry F., Kierlik E., Rosinberg M. L. and Tarjus G., *Phys. Rev. E* , **73** (2006) 041511.